COMPDYN 2011
ECCOMAS Thematic Conference on
Computational Methods in Structural Dynamics and Earthquake Engineering
M. Papadrakakis, M. Fragiadakis, V. Plevris (eds.)
Corfu, Greece, 25-28 May 2011

PIEZOELECTRIC TORSIONAL SENSORS AND ACTUATORS - A COMPUTATIONAL STUDY

Christian Zehetner[1], Markus Zellhofer[1] and Michael Krommer[2]

[1]Linz Center of Mechatronics
Linz, Austria
e-mail: {christian.zehetner, markus.zellhofer}@lcm.at

[2] Institute for Technical Mechanics
Johannes Kepler University, Linz, Austria
e-mail: michael.krommer@jku.at

Keywords: Torsion, piezoelectric rod, piezoelectric actuation, piezoelectric sensor, macro fiber composites

Abstract. *This paper concerns a computational study on the realization of piezoelectric torsional actuators and sensors. Exemplarily, a rod with rectangular solid cross-section is considered consisting of a linear elastic substrate material on which orthotropic piezoelectric layers are bonded. On the one hand side, piezoelectric actuation is obtained by applying voltage to the electrodes of the piezoelectric layer. Secondly, the layers can be used as sensors by measuring the voltage on the electrodes which is caused by external torsional loads. Three material types are compared for possible realisations: ammonium dihydrogen phosphate (ADP) and two types of macro fiber composites (MFC). In the framework of Saint Venant's theory of torsion, the actuator and sensor equations are formulated: The actuating torsional moment is proportional to the applied voltage, and the sensor voltage is proportional to the torsional angle. Finally, the results are validated by means of three-dimensional Finite Element computations.*

1 INTRODUCTION

Recently, interest in active vibration compensation using piezoelectric materials has gained more and more. Possible applications can be found for instance in the fields of robotics and light-weight structures. Piezoelectric layers can either be integrated into structures, or applied on the surfaces of structures. Such layers can be used as sensors and actuators, utilizing the direct and converse piezoelectric effect, respectively, [1].

The topic of this paper is the application of piezoelectric materials for sensing and actuation of torsional rod vibrations. Exemplarily, a rod of rectangular cross-section made of aluminium is considered which is subject to an external torsional couple. On the top and bottom of the rod, piezoelectric layers are attached, such that a sandwich structure is obtained. Each layer can be used as a sensor by measuring the voltage on the electrodes, or as an actuator by prescribing the voltage. The main scope is the derivation of the sensor and actuator equations, and to perform numerical investigations in order to find a suitable configuration for an experimental setup.

Torsional actuation and sensing is either based on the piezoelectric extension or on the shear mode. In the first case, torsional actuation is obtained by piezoelectric normal strains acting at an angle of 45^o degrees to the rod axis, c.f. Park and Chopra [2]. In the second case, piezoelectric shear strains cause a resulting actuating torque, [3]-[9]. On the other hand, in torsional sensors the strains corresponding to the piezoelectric mode cause the sensor voltage at the electrodes. In this paper two types of materials are investigated: (a) Shear mode: Piezoceramic material ammonium dihydrogen phosphate (ADP) and (b) Extension mode: Macro fiber composites (MFC) consisting of lead zirconate titanate (PZT) fibers embedded within an epoxy-substrate. Two types of MFCs are compared utilizing eiter the transversal d_{31}-effect or the longitudinal d_{33}-effect of the PZT fibers. For the MFC transduceres effective homogenized material properties are used, which have been obtained by applying mixing rules according to Deraemaeker et al. [10].

In order to investigate the influence of piezoelectricity on torsion, Saint Venant's theory has been extended by Zehetner [5] and Zehetner and Krommer [7]. The main extension is the consideration of the additional cross-sectional warping caused by piezoelectric strains. In this paper, the theory is adapted for studying the behaviour of the three materials mentioned above. It turns out that for the three configurations the sensor and actuator equations only differ with respect to some coefficients referring to the material properties. It also turns out that for an experimental realization MFCs are more practicable because of higher sensitivity and efficiency of actuation. Finally, the theoretical results are validated by means of three-dimensional Finite Element computations performed with *ANSYS* and *ABAQUS* showing a good coincidence.

2 PIEZOELECTRIC SHEAR ACTUATORS AND SENSORS

In this paper two kinds of materials suitable for torsional sensing and actuation are investigated: Figure 1a shows a homogenous layer made of the piezoceramic ammonium dihydrogen phosphate (ADP), z is the thickness direction, and x is the axial direction of the rod. The second type of material is shown in Figure 1b, a macro fiber composite (MFC) consisting of piezoceramic fibers (lead zirconate titanate, PZT) which are embedded into an epoxy-substrate at an angle of 45^o with respect to the axial direction x of the rod.

The compliance matrices $\boldsymbol{S}$ of the two materials are stated in Eq. (1). In layers made of ADP, the shear strains correspond to the shear stresses only. The same behavior is obtained for MFC's, if the coordinate frame coincides with the axes of material symmetry. On the contrary, for the investigated case with a ply angle of 45^o, the shear strains are coupled to normal stresses

by the compliance components S_{16} and S_{36}.

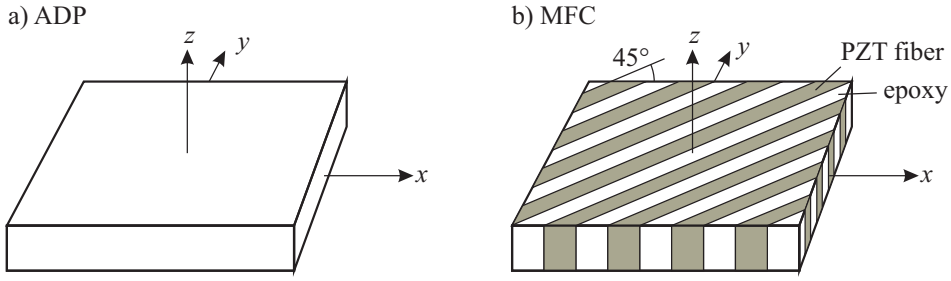

Figure 1: Piezoelectric materials

a) ADP b) MFC

$$\boldsymbol{S} = \begin{bmatrix} S_{11} & S_{12} & S_{13} & 0 & 0 & 0 \\ S_{12} & S_{11} & S_{13} & 0 & 0 & 0 \\ S_{13} & S_{13} & S_{33} & 0 & 0 & 0 \\ 0 & 0 & 0 & S_{55} & 0 & 0 \\ 0 & 0 & 0 & 0 & S_{55} & 0 \\ 0 & 0 & 0 & 0 & 0 & S_{66} \end{bmatrix}, \quad \boldsymbol{S} = \begin{bmatrix} S_{11} & S_{12} & S_{13} & 0 & 0 & S_{16} \\ S_{12} & S_{11} & S_{13} & 0 & 0 & S_{16} \\ S_{13} & S_{13} & S_{33} & 0 & 0 & S_{36} \\ 0 & 0 & 0 & S_{55} & S_{45} & 0 \\ 0 & 0 & 0 & S_{45} & S_{55} & 0 \\ S_{16} & S_{16} & S_{36} & 0 & 0 & S_{66} \end{bmatrix}. \quad (1)$$

Three configurations are considered as shown in Figure 2: (a,b) A layer made of ADP or MFC type 1 (d_{31}-effect) is polarized in thickness direction, and the electrodes are bonded on the top and bottom surfaces, (c) A layer made of MFC type 2 (d_{33}-effect) is polarized in longitudinal direction of the fibers, and the electrodes are normal to this direction.

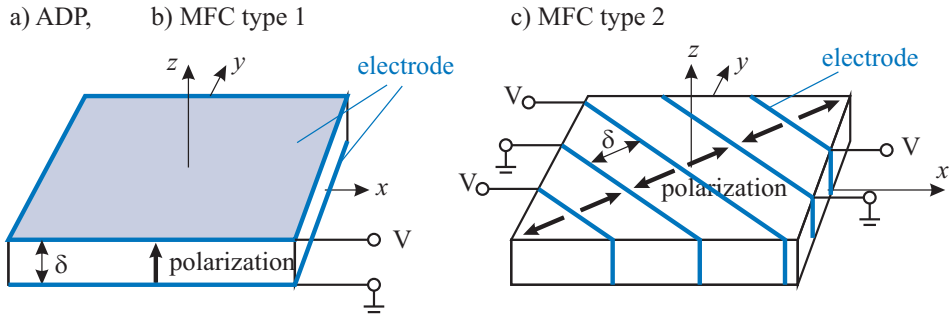

Figure 2: Electrodes and polarization direction

The matrices $\boldsymbol{d}$ of piezoelectric coefficients d_{ij} for the three configurations are specified in Eq. (2). In layers made of ADP only piezoelectric shear strains are induced, such that pure torsional actuation is possible. On the contrary, in MFC's also normal eigenstrains arise, which can excite elongation and bending modes of the rod. In the following, the bending mode is avoided due to a symmetrical set-up, and the elongation is neglected.

a) ADP b) MFC type 1 c) MFC type 2

$$\boldsymbol{d} = \begin{bmatrix} 0 & 0 & 0 \\ 0 & 0 & 0 \\ 0 & 0 & 0 \\ d_{25} & 0 & 0 \\ 0 & d_{25} & 0 \\ 0 & 0 & d_{36} \end{bmatrix}, \quad \boldsymbol{d} = \begin{bmatrix} 0 & 0 & d_{13} \\ 0 & 0 & d_{13} \\ 0 & 0 & d_{33} \\ d_{25} & d_{15} & 0 \\ d_{15} & d_{25} & 0 \\ 0 & 0 & d_{36} \end{bmatrix}, \quad \boldsymbol{d} = \begin{bmatrix} d_{11} & d_{12} & 0 \\ d_{12} & d_{11} & 0 \\ d_{13} & d_{13} & 0 \\ 0 & 0 & d_{35} \\ 0 & 0 & d_{35} \\ d_{16} & d_{16} & 0 \end{bmatrix}. \quad (2)$$

3 TORSION OF PIEZO-LAMINATED RODS

Figure 3 shows the cross-section of a laminated rod with length L, width B and total height H. The rod consists of an isotropic aluminum layer with height h on which two piezoelectric layers with height h_L are ideally bonded. The rod is subject to the external torsional couple M_x^e. A Cartesian coordinate system is introduced such that the x-axis represents the longitudinal axis of the rod, and the axes y and z form the cross-sectional plane. The cross-sectional area of the piezoelectric layers is denoted as A_L, the interface between the layers i and j by ∂I_{ij}, A is the total cross-sectional area, and ∂A the boundary of the cross-section.

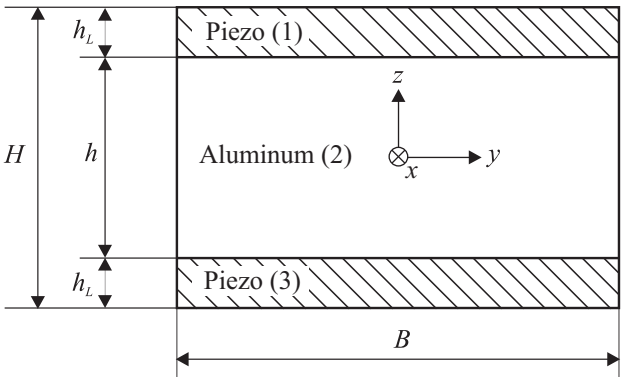

Figure 3: Cross-section of the laminated rod

3.1 Kinematical assumptions

According to Saint Venant's theory of torsion, the elastic deformation of the rod is composed of a rigid-body rotation of the cross-section about the torsional angle $\chi = \chi(x,t)$ and an axial displacement due to cross-sectional warping. It has been shown by Zehetner [5] that under the presence of piezoelectric shear strains the displacement components can be expressed by

$$u_x = \chi'\varphi + \phi^0, \quad u_y = -z\chi, \quad u_z = y\chi, \tag{3}$$

where $\varphi = \varphi(y,z)$ is Saint Venant's warping function, and the additional warping function $\phi^0 = \phi^0(y,z,t)$ represents the additive influence of the piezoelectric strains on the axial displacement. In order to obtain continuity at the interfaces, the warping functions have to satisfy the compatibility relations

$$\partial I_{ij}: \quad [\![\varphi(y,z)]\!] = 0, \quad [\![\phi^0(y,z)]\!] = 0, \tag{4}$$

where the notation $[\![\cdot]\!]$ stands for the jump of the respective quantity at the interface ∂I_{ij}. Note that due to the interface conditions the additional warping function is defined for the whole cross-section. With Eq. (3) and the assumption that $\chi'' = 0$ in case of unconstrained warping, the only non-vanishing linearized strain components are the shear angles

$$\gamma_{xz} = \chi'\left(\frac{\partial\varphi}{\partial z} + y\right) + \frac{\partial\phi^0}{\partial z}, \quad \gamma_{xy} = \chi'\left(\frac{\partial\varphi}{\partial y} - z\right) + \frac{\partial\phi^0}{\partial y}. \tag{5}$$

3.2 Constitutive Relations

The constitutive relations for the considered materials have been stated in section 2. Assuming, that the piezoelectric layers are thin, the normal stress σ_{zz} in thickness and the shear stress τ_{yz} are neglected, such that the mechanical consitutive relations can be written in the generalized form

$$\begin{bmatrix} \sigma_{xx} \\ \sigma_{yy} \\ \tau_{xz} \\ \tau_{xy} \end{bmatrix} = \begin{bmatrix} Q_{11} & Q_{12} & 0 & Q_{16} \\ Q_{12} & Q_{11} & 0 & Q_{16} \\ 0 & 0 & Q_{55} & 0 \\ Q_{16} & Q_{16} & 0 & Q_{66} \end{bmatrix} \left(\begin{bmatrix} \varepsilon_{xx} \\ \varepsilon_{yy} \\ \gamma_{xz} \\ \gamma_{xy} \end{bmatrix} - \begin{bmatrix} \varepsilon^0_{xx} \\ \varepsilon^0_{yy} \\ \gamma^0_{xz} \\ \gamma^0_{xy} \end{bmatrix} \right), \tag{6}$$

where Q_{ij} are the coefficients of the effective stiffness matrix, ε^0_{ii} and γ^0_{ij} are piezoelectric eigenstrains. From the kinematical assumptions in section 3.1 follows that $\varepsilon_{xx} = \varepsilon_{yy} = 0$, such that the constitutive equations reduce to

$$\tau_{xz} = Q_{55}(\gamma_{xz} - \gamma^0_{xz}), \qquad \tau_{xy} = Q_{66}(\gamma_{xy} - \bar{\gamma}^0_{xy}). \tag{7}$$

Note that the constitutive relations for the isotropic substrate (aluminium) follows from Eq. (7) by setting $\gamma^0_{xz} = \gamma^0_{xy} = 0$ and $Q_{55} = Q_{66} = G$. For the piezoelectric materials in section 2 we obtain the effective shear moduli

$$Q_{55} = S^{-1}_{55}, \quad Q_{66} = \begin{cases} S^{-1}_{66} & \text{for ADP,} \\ (S_{11} + S_{12})(S_{11}S_{66} - S^2_{16} + S_{12}S_{66})^{-1} & \text{for MFC.} \end{cases} \tag{8}$$

For the considered piezoelectric materials the effective eigenstrains can be expressed by

$$\gamma^0_{xz} = 0, \qquad \bar{\gamma}^0_{xy} = d_{xy}E_{\parallel}, \tag{9}$$

where $E_{\parallel}$ is the component of the electric field parallel to the polarization direction, and d_{xy} is the effective piezoelectric coefficient, which depends on the material type, i.e.

$$d_{xy} = \begin{cases} d_{36} & \text{for ADP,} \\ d_{36} - 2d_{31}S_{16}(S_{11} + S_{12})^{-1} & \text{for MFC type 1,} \\ \sqrt{2}d_{16} - \sqrt{2}(d_{11} + d_{12})S_{16}(S_{11} + S_{12})^{-1} & \text{for MFC type 2.} \end{cases} \tag{10}$$

Assuming that the distance δ between the electrodes is relatively small, the parallel electric field component is proportional to the applied voltage V, but the normal component vanishes,

$$E_{\parallel} = \frac{V}{\delta}, \quad E_{\perp} = 0. \tag{11}$$

The electrical constitutive relations for the piezoelectric materials are given by

$$D_{\parallel} \;\; = \;\; \eta_{\parallel}(E_{\parallel} - E^0_{\parallel}), \tag{12}$$

where $D_{\parallel}$ is the dielectric displacement component in direction of the polarization, $\eta_{\parallel}$ the permittivity, and $E^0_{\parallel}$ the electric eigenfield representing the direct piezoelectric effect,

$$E^0_{\parallel} = -\frac{d_{xy}}{\eta_{\parallel}}\tau_{xy}. \tag{13}$$

Inserting Eqs. (5), (9) and (11) into Eq. (7) yields the shear stresses in the piezoelectric layers as

$$\tau_{xz} = Q_{55}\left[\left(\frac{\partial\varphi}{\partial z} + y\right)\chi' + \frac{\partial\phi^0}{\partial z}\right],$$
$$\tau_{xy} = Q_{66}\left[\left(\frac{\partial\varphi}{\partial y} - z\right)\chi' + \frac{\partial\phi^0}{\partial y} - \frac{d_{xy}}{\delta}V\right]. \tag{14}$$

Note that the stresses in the isotropic substrate layer are obtained by setting $Q_{55} = Q_{66} = G$ and $V = 0$. Integrating over the cross-sectional area yields the internal torsional moment

$$M_x = C_{11}\chi' - M_x^a \tag{15}$$

with the torsional stiffness C_{11} and the actuating torsional moment M_x^a,

$$C_{11} = \int_A \left[Q_{55}\left(\frac{\partial\varphi}{\partial z} + y\right)y - Q_{66}\left(\frac{\partial\varphi}{\partial y} - z\right)z\right]\,\mathrm{dA}, \tag{16}$$

$$M_x^a = -\int_A \left(Q_{55}\frac{\partial\phi^0}{\partial z}y - Q_{66}\frac{\partial\phi^0}{\partial y}\right)\mathrm{d}A - 2V\int_{A_L} Q_{66}\frac{d_{xy}}{\delta}z\,\mathrm{dA}. \tag{17}$$

3.3 Warping functions

Inserting Eq. (14) into the equilibrium equations of elastostatics,

$$\frac{\partial\tau_{xy}}{\partial y} + \frac{\partial\tau_{xz}}{\partial z} = 0, \quad \partial A:\ \tau_n = 0, \quad \partial I_{ij}:\ [\![\tau_n]\!] = 0, \tag{18}$$

where τ_n is the projection of the shear stress on the outer normal of the boundary and interface, yields boundary value problems for the warping functions φ and ϕ^0, c.f. Zehetner [5]. For the cross-section in Figure 3 the Saint Venant warping function φ follows to

$$Q_{66}\frac{\partial^2\varphi}{\partial y^2} + Q_{55}\frac{\partial^2\varphi}{\partial z^2} = 0, \tag{19}$$
$$\partial A_h:\ \frac{\partial\varphi}{\partial z} = -y, \quad \partial A_v:\ \frac{\partial\varphi}{\partial y} = z, \quad \partial I_{ij}:[\![Q_{55}\frac{\partial\varphi}{\partial z}]\!] = 0, \quad [\![\varphi]\!] = 0,$$

where ∂A_h denotes the horizontal boundary at the top and bottom, and ∂A_v the vertical boundary. Solutions of Eq. (19) are given in Rand and Rovenski [11]. A similar boundary value problem is obtained for the additional warping function. Using the separation

$$\phi_0(y, z, V(t)) = \frac{d_{xy}}{\delta}V(t)\bar{\phi}^0(y, z) \tag{20}$$

yields the boundary value problem

$$Q_{66}\frac{\partial^2\bar{\phi}^0}{\partial y^2} + Q_{55}\frac{\partial^2\bar{\phi}^0}{\partial z^2} = 0, \tag{21}$$
$$\partial A_h:\ \frac{\partial\bar{\phi}^0}{\partial z} = 0, \quad \partial A_v:\ \frac{\partial\bar{\phi}^0}{\partial y} = 1, \quad \partial I_{ij}:\ [\![Q_{55}\frac{\partial\bar{\phi}^0}{\partial z}]\!] = 0, \quad [\![\bar{\phi}^0]\!] = 0.$$

A solution of Eq. (21) has been given in Zehetner [5]. Note that $\varphi(y, z)$ and $\bar{\phi}^0(y, z)$ only depend on geometric and material properties.

4 SENSOR AND ACTUATOR EQUATIONS

Inserting Eq. (20) into Eq. (17) yields the actuator equation

$$M_x^a(t) = c_A V(t), \tag{22}$$

i.e. the actuating moment is proportional to the applied voltage with the actuator constant

$$c_A = \int_A \left[Q_{55} \frac{\partial \bar{\phi}^0}{\partial z} y - Q_{66} \frac{\partial \bar{\phi}^0}{\partial y}\, z \right] \mathrm{d}A - 2 \int_{A_L} Q_{66} \frac{d_{xy}}{\delta}\, z \, \mathrm{d}A. \tag{23}$$

Following the strategy presented by Zehetner and Krommer [7] yields the sensor equation

$$V(t) = -c_S\, \chi_L(t), \tag{24}$$

i.e. the measured voltage is proportional to the tip torsional angle with the sensor constant

$$c_S = \frac{d_{xy} Q_{66} \delta}{L} \frac{\int\limits_{A_{el}} \left(\frac{\partial \varphi}{\partial y} - z \right) \mathrm{d}A}{\int\limits_{A_{el}} \left[\left(\frac{\partial \bar{\phi}^0}{\partial y} - 1 \right) d_{xy}^2 Q_{66} + \eta_{\|} \right] \mathrm{d}A}. \tag{25}$$

Note that the actuator constant depends on cross-sectional properties only, but the sensor constant is a function of the rod length.

5 NUMERICAL EXAMPLES

5.1 Results of rod theory

In this section the expressions for torsional stiffness, actuator and sensor constants given in Eqs. (16), (23) and (25) are evaluated using the numerical values of table 1, $\eta_0 = 8.854 \cdot 10^{-12}\ \mathrm{F/m}$ is the permittivity of vacuum. The results are compared in table 2. The highest actuator constant is obtained for MFC type 2, and the highest sensor constant for ADP.

property	unit	ADP	MFC type 1	MFC type 2
Q_{55}	N/m^2	$8.6207 \cdot 10^9$	$2.3059 \cdot 10^9$	$2.2959 \cdot 10^9$
Q_{66}	N/m^2	$6.0241 \cdot 10^9$	$4.2484 \cdot 10^9$	$3.8188 \cdot 10^9$
d_{xy}	C/N	$5.17 \cdot 10^{-11}$	$1.7234 \cdot 10^{-10}$	$5.1495 \cdot 10^{-10}$
$\eta_{\|}/\eta_0$	1	15.4	307.12	307.12

Table 1: Material properties

constant	unit	ADP	MFC type 1	MFC type 2
C_{11}	Nm^2/rad	67.31	63.41	62.52
c_A	Nm/V	$8.5827 \cdot 10^{-5}$	$2.002 \cdot 10^{-4}$	$5.4028 \cdot 10^{-4}$
c_S	V/rad	$3.5443 \cdot 10^4$	$3.8773 \cdot 10^3$	$1.5235 \cdot 10^4$

Table 2: Rod Theory: Sensor and actuator constants

5.2 Finite Element Results

In the following these results of rod theory are verified by means of three dimensional Finite Element computations using the model presented in Zehetner [5]. The model has been implemented within *ABAQUS* and *ANSYS*. The following steps have been performed:

1. The torsional stiffness C_{11} is obtained by applying an external torsional couple $M_x^e = 100\ \mathrm{Nm}$ to the rod and evaluating the torsional tip angle χ_L for $V = 0$. The stiffness is then obtained from Eq. (15),
$$C_{11} = \frac{M_x^e L}{\chi_L}. \tag{26}$$

2. For evaluating the actuator constant c_A the external torsional couple is set to $M_x^e = 0$ and the voltage $V = 100\ \mathrm{V}$ is prescribed. Equation (15) yields
$$c_A = \frac{C_{11}}{V}\frac{\chi_L}{L}. \tag{27}$$

3. The sensor constant c_S is obtained by applying an external torsional couple M_x^e to the rod and evaluating the torsional angle and the sensor voltage V. From Eq. (24) follows that
$$c_S = \frac{V}{\chi_L}. \tag{28}$$

The deformed rod for load case 2 with an actuator voltage of $V = 100\ \mathrm{V}$ is shown in Figure 4, where the displacements have been scaled by a factor of 1000. The figure shows that the largest actuation is obtained for MFC type 2.

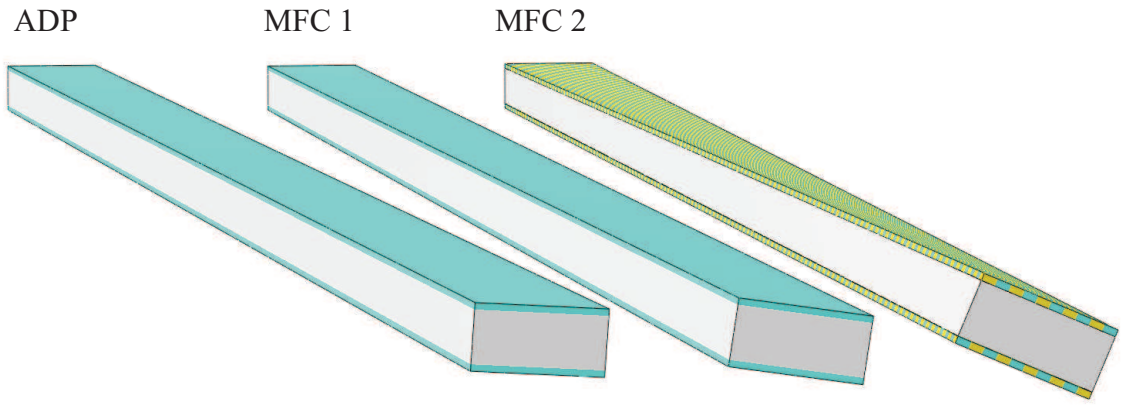

Figure 4: Deformed rod, displacements scaled by a factor of 1000

The results for Eqs. (26)-(28) obtained with *ABAQUS* and *ANSYS* are shown in Tables 3 and 4, respectively.

load case	constant	unit	ADP	MFC type 1	MFC type 2
1	M_x^e	Nm	0.01	0.01	0.01
stiffness	V	V	0	0	0
	χ_L	rad	$7.356 \cdot 10^{-5}$	$7.852 \cdot 10^{-5}$	$7.9380 \cdot 10^{-5}$
	C_{11}	Nm^2/rad	67.97	63.68	62.99
2	M_x^e	Nm	0	0	0
actuator	V	V	100	100	100
constant	χ_L	rad	$6.315 \cdot 10^{-5}$	$1.496 \cdot 10^{-4}$	$4.2620 \cdot 10^{-4}$
	c_A	Nm/V	$8.585 \cdot 10^{-5}$	$1.904 \cdot 10^{-4}$	$5.3691 \cdot 10^{-4}$
3	M_x^e	Nm	0.01	0.01	0.01
sensor	V	V	2.543	0.314	1.209
constant	χ_L	rad	$7.196 \cdot 10^{-5}$	$7.805 \cdot 10^{-5}$	$7.423 \cdot 10^{-5}$
	c_S	V/rad	$3.53 \cdot 10^4$	$4.023 \cdot 10^3$	$1.629 \cdot 10^4$

Table 3: Results of the ABAQUS analysis

load case	constant	unit	ADP	MFC type 1	MFC type 2
1	M_x^e	Nm	0.01	0.01	0.01
stiffness	V	V	0	0	0
	χ_L	rad	$7.39 \cdot 10^{-5}$	$7.842 \cdot 10^{-5}$	$7.538 \cdot 10^{-5}$
	C_{11}	Nm^2/rad	67.66	63.76	66.33
2	M_x^e	Nm	0	0	0
actuator	V	V	100	100	100
constant	χ_L	rad	$6.3 \cdot 10^{-5}$	$1.534 \cdot 10^{-4}$	$4.084 \cdot 10^{-4}$
	c_A	Nm/V	$8.53 \cdot 10^{-5}$	$1.956 \cdot 10^{-4}$	$5.418 \cdot 10^{-4}$
3	M_x^e	Nm	0.01	0.01	0.01
sensor	V	V	2.53	0.309	1.157
constant	χ_L	rad	$7.24 \cdot 10^{-5}$	$7.77 \cdot 10^{-5}$	$7.08 \cdot 10^{-5}$
	c_S	V/rad	$3.494 \cdot 10^4$	$3.976 \cdot 10^3$	$1.634 \cdot 10^4$

Table 4: Results of the ANSYS analysis

The results of rod theory in Section 5.1 are confirmed: The highest actuator constant is obtained for MFC type 2, and the highest sensor constant for ADP. The slight differences between *ABAQUS* and *ANSYS* result from some minor discrepancies in the Finite Element models. A better adjustment of the models is a topic for further investigations.

5.3 Comparison of rod theory and FEM

Finally, the results of rod theory and Finite Element computations are compared in Figure 5. The relative difference of Finite Element and rod theory solutions are shown in Table 5.

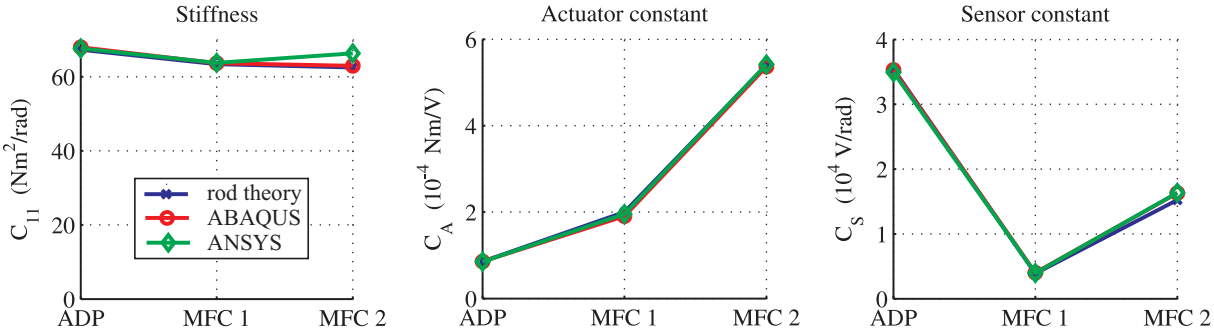

Figure 5: Comparison of the results for C_{11}, c_A and c_S

constant		ADP	MFC type 1	MFC type 2
C_{11}	*ABAQUS*	1.0 %	0.4 %	0.8 %
	ANSYS	0.5 %	0.6 %	6.1 %
C_A	*ABAQUS*	0.0 %	4.9 %	0.6 %
	ANSYS	0.6 %	2.3 %	0.3 %
C_S	*ABAQUS*	0.3 %	3.8 %	6.9 %
	ANSYS	1.4 %	2.5 %	7.3 %

Table 5: Comparison of theory and Finite Element solutions: Relative difference

The maximum difference of 7.3% is obtained for the sensor constant of MFC type 2. The differences in Table 5 result from the assumptions of the presented rod theory, e.g. the kinematical assumptions and the neglect of some coupling terms. All in all Figure 5 shows a good coincidence of the results, such that the presented rod theory can be utilized for finding a suitable configuration for the planned experimental verification.

6 CONCLUSIONS

In this paper it has been shown how three kinds of piezoelectric materials can be used for actuating and sensing of torsional vibrations. An extension of Saint Venant's theory of torsion has been used to derive sensor and actuator equations. A numerical evaluation has shown high sensitivity of the investigated configurations, but relative small efficiency for actuation. The highest sensor constant is obtained for the ADP layer, and the highest actuator constant for MFC type 2.

ACKNOWLEDGEMENTS

Support of the authors from the Austrian Center of Competence in Mechatronics (ACCM) and of M.Krommer & M.Zellhofer from the Austrian Science Fund (FWF Translational project L441-N41 *Sensor Systems for Structural and Health Monitoring*) is gratefully acknowledged.

REFERENCES

[1] W.P. Mason W.P, Piezoelectricity, its history and applications. *Journal of the Acoustical Society of America*, **6**, 1561-1566, 1981.

[2] C. Park, I. Chopra, Modeling piezoceramic actuation of beams in torsion. *AIAA Journal*, **34**, 2582-2589, 1996.

[3] C. Sung, V.V. Varadan, X. Bao, V.K. Varadan, Active torsional vibration control experiments using shear-type piezoceramic sensors and actuators. *Journal of Intelligent Materials Systems and Structures*, **4**, 436-442, 1994.

[4] L.R. Centolanza, E.C. Smith, B. Munsky, Induced-shear piezoelectric actuators for rotor blade trailing edge flaps. *Smart Materials and Structures*, **11**, 24-35, 2002.

[5] Ch. Zehetner, Compensation of Torsion in Rods by Piezoelectric Actuation, *Archive of Applied Mechanics*, **78**, 921-933, 2008.

[6] Ch. Zehetner, Compensation of torsional vibrations in rods by piezoelectric actuation. *Acta Mechanica*, **207**, 121-133, 2009.

[7] Ch. Zehetner, M. Krommer, Control of torsional vibrations by piezoelectric sensors and actuators, *Proceedings of COMPDYN 2009*, M. Papadrakakis, N.D. Lagaros, M. Fragiadakis (eds.), Rhodes, Greece, June 22-24, 2009.

[8] Ch. Zehetner, M.Krommer, Control of torsional vibrations in piezolaminated rods, *Structural Control and Health Monitoring*, accepted for publication, 2011.

[9] P. Berik, A. Benjeddou, Piezoelectric d_{15} shear response-based torsion actuation mechanism: An experimental benchmark and its 3D finite element simulation. *International Journal of Smart and Nano Materials*, **1**, 224-235, 2010.

[10] A. Deraemaeker, H. Nasser, A. Benjeddou, A. Preumont, Mixing Rules for the piezoelectric properties of macro fiber composites, *Journal of Intelligent Material Systems and Structures*, **20**, 1475-1482, 2009.

[11] O. Rand, V. Rovenski, *Analytical Methods in Anisotropic Elasticity*, Birkhäuser, Boston, 2005.